# Study of MDM2 Binding to p53-Analogues: Affinity, Helicity, and Applicability to Drug Design

Ori Kalid* and Nir Ben-Tal

Department of Biochemistry, George S. Wise Faculty of Life Sciences, Tel-Aviv University, Ramat Aviv 69978, Israel

MDM2 is a key regulator of the p53 tumor-suppressor protein. Here we study the effect of modifications of a p53 N-terminal fragment on its binding to MDM2, using implicit-solvent MD and MM-GB/SA calculations. We provide interpretation of existing experimental data and predict the effect of mutations on binding. Notably 1) We analyze the effect of regulatory phosphorylations at Ser/Thr residues and suggest that a balance between favorable electrostatics and desolvation penalties determines the effect of phosphorylation; 2) We compare the helical stability in solution of p53 alanine mutants and propose a helix stabilizing role for several residues involved in hydrogen bonding and hydrophobic packing; 3) We obtain good correlations between calculated and experimental affinities for a set of peptidomimetic inhibitors, both alone and in combination with p53 analogues, demonstrating potential applicability to drug design. From the technical aspect, protocol optimization and selection of simulation tools are addressed in detail. To the best of our knowledge this is the first published example of MM-GB/SA calculations utilizing a conformational ensemble generated with implicit solvent MD. Our results suggest that this highly efficient variant of classical explicit-solvent MM-GB/SA may be used for studying protein−protein interactions and for the design of peptidomimetic drugs.

## INTRODUCTION

The tumor-suppressor protein p53 leads to cell-cycle arrest and apoptosis in response to cellular damage, acting mostly as a transcription factor. While not required for normal growth and development, p53 is critical for the prevention of tumor development. Defects in the p53 pathway are found in most human cancers, and p53 knockout mice show a dramatic increase in tumor occurrence.[1] Due to its powerful inhibition of cell growth, p53 function must be tightly regulated in normal human cells. This is accomplished by multiple control mechanisms, the most important of which seem to be at the mature protein level, including regulation of protein stability, cellular localization, post-translational modifications, and conformational changes affecting its ability to bind DNA.[1] One of the central components in the regulation of p53 is the p53-interacting protein MDM2. MDM2 is in itself a transcriptional target of p53 and so establishes a negative feedback loop in which p53 promotes the expression of its own down regulator. MDM2 amplification has been described in certain tumor types, including some sarcomas and brain cancer. In mice, homozygous deletion of MDM2 leads to apoptosis in the embryo and very early embryonic lethality. This effect is countered by a simultaneous knockout of p53. MDM2 interacts with the N-terminal domain of p53 (residues 15−29), containing the major p53 transcription activation domain. This interaction directly interferes with p53's ability to contact transcriptional coactivator proteins. In addition, MDM2 also functions as a ubiquitin ligase for both p53 and itself and so modulates the half-life of p53.[1]

The interaction of p53 with MDM2 has been studied extensively. The following section highlights selected studies from recent years, emphasizing the diversity in acquisition methods, discussing interpretability, and assessing compatibility between the studies.

One of the first studies, by Picksley et al., tested the effect of alanine mutations on the MDM2 binding capacity of p53(16−25). Using an ELISA binding assay they showed that residues 18−23 (TFSDLW) are all critical for binding.[2] A study by Lin et al. tested the ability of p53 mutants to bind MDM2 using a single concentration immunoprecipitation assay.[3] This study showed that mutations Leu22Gln and Trp23Ser reduced MDM2 binding to 56% and 22%, respectively, while the double mutant retained only 2% of the *wt* activity. However, given only single concentration data, the actual effect on binding affinity is not clear.

In a later study, Bottger et al. described a series of MDM2 binding peptides selected from a phage display library.[4] This analysis was later extended to a synthetic library of peptides derived from the initial discovery.[5] Bottger et al. characterized the ability of these peptides to inhibit p53 binding to MDM2 using three different ELISA formats (peptide-ELISA, MDM2-ELISA, and p53-ELISA, according to the immobilized species). A systematic alanine scan of the optimal phage-derived 12-mer peptide revealed that Phe19 and Trp23 are critical for binding, all substitutions leading to complete loss of activity. (The paper also mentions a similar affect on the *wt* p53, but the data are not shown). Leu26 could only be replaced by Ile, Met, and Val albeit with 3−5-fold reduction in potency. In the crystal structure of p53 with

* Corresponding author phone: ++972-3-640-9804; mobile: ++972-54-2233074; fax: ++972-3-640-6834; e-mail: orikalid@gmail.com.
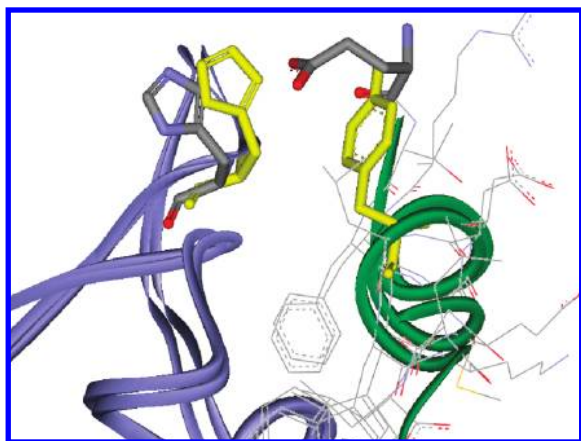
**Figure 1.** Preference for Tyr at position 22: Superimposition of the 1YCR and 1T4F crystal structures. Green ribbon: bound peptide ligand. Blue ribbon: MDM2. In the 1T4F complex of MDM2 with the Bottger 9-mer peptide, Try22 (sticks, yellow) is involved in T-shaped aromatic interactions with His73 (sticks, yellow). However, in the *wt* complex, Glu17 (sticks, colored by element) occupies that same space, making His73 (sticks, colored by element) significantly less accessible to interactions with position 22. Therefore the preference for aromatic interactions may be unique to the Bottger peptides, which all lack Glu17 (the longer analogues have Pro residue at this position).

human MDM2 (hence MDM2) (1YCR[6]) Phe19, Trp23, and Leu26 form the anchoring interactions of p53 to MDM2, explaining the intolerance for substitutions at these positions. With regard to the importance of Leu26, Bottger et al. also measured a significantly lower affinity for p53(18−25), 50−140-fold weaker than p53(16−27).[5] This is in contrast to the results of Picksley et al. showing increased potency for p53(18−25) over p53(15−30).[2] The source for this inconsistency is unclear. Additionally, Bottger et al. demonstrated a 2-fold increase in activity for p53(16−27)Leu22Tyr over *wt*. For the phage derived peptide, position 22 (numbering according to *wt* sequence) was shown to prefer all aromatic residues over the *wt* leucine. In the 1YCR crystal structure, Leu22 is involved in vdW interactions with MDM2 residues Lys94 and His73. Superimposition of the crystal structures of MDM2 in complex with p53(15−29) (1YCR) and with a 9-mer peptide from the Bottger study (1T4F[7]) suggests that the preference for aromatics may be exclusive to the Bottger peptides, which lack Glu17 (the longer analogues have a proline at this position). In the 9-mer complex Try22 is involved in T-shaped aromatic interactions with His73 of MDM2. However, in the *wt* complex Glu17 occupies the same region, making His73 significantly less accessible to interactions with position 22 (Figure 1). Quantitative data could not be extracted from this study due to the variability between the three ELISA assays.

A study by Lai et al. probed the effects of phosphorylations and peptide length on the p53-MDM2 interaction using a fluorescence anisotropy competition assay.[8] Lai et al. showed that phosphorylation of either Ser15, Ser20, or a dual phosphorylation of both had a minor effect on peptide affinity (Table 1), while phosphorylation of Thr18 alone or in combination with Ser15 led to a ∼20-fold reduction in binding. They also showed that the affinity of the 35 residue long peptide p53(1−35) (700 nM) is identical to that of the shorter p53(10−29) (750 nM), in accordance with the crystal structure of the p53-MDM2 complex (1YCR[6]), which

**Table 1.** Collection of p53 Derivatives Used in the Present Analysis[a]

|  | $K_d$ (µM) | error (µM) |
|---|---|---|
| Full Length Peptides | | |
| p53(1−35)[b] | 0.7 | 0.1 |
| p53(7−36)[c] | 0.121 | 0.001 |
| p53(12−30)[c] | 0.229 | 0.012 |
| p53(10−29)[b] | 0.75 | 0.1 |
| p53(15−29)[d] | 0.575 | 0.019 |
| PMD13: p53(15−29)F19Nal[d] | 0.84 | 0.06 |
| PMD14: p53(15−29)W23Nal[d] | 1.35 | 0.4 |
| PMD16: p53(15−29)L26F[d] | 1.27 | 0.12 |
| PMD27: p53(15−29)T18S[d] | 0.47 | 0.06 |
| p53(12−30)D21A[c] | 0.17 | 0.007 |
| p53(12−30)W23L[c] | 43 | 2 |
| p53(12−30)L26I[c] | 0.209 | 0.014 |
| p53(12−30)P27S[c] | 0.0047 | 0.0006 |
| Short Peptides | | |
| p53(17−26)[b] | 0.05 | 0.01 |
| p53(18−26)[b] | 0.07 | 0.01 |
| p53(19−26)[b] | 0.8 | 0.1 |
| p53(19−25)[b] | 150 | 50 |
| PMD2: p53(17−26)[d] | 0.046 | 0.007 |
| PMD3: p53(17−26)F19Nal[d] | 0.053 | 0.002 |
| PMD4: p53(17−26)W23Nal[d] | 0.93 | 0.23 |
| PMD22: p53(19−26)[d] | >5 | |
| PMD23: p53(17−26)F19MePhe[d] | 1.8 | 0.2 |
| PMD25: p53(18−26)[d] | 0.07 | 0.009 |
| Phosphorylated Peptides | | |
| p53(10−29)pS15[b] | 1.29 | 0.15 |
| p53(10−29)pS20[b] | 0.55 | 0.1 |
| p53(10−29)pS15/pS20[b] | 0.63 | 0.1 |
| p53(10−29)pT18[b] | 11 | 1 |
| p53(10−29)pS15/pT18[b] | 14 | 1 |
| p53(15−29)pS15[d] | 0.27 | 0.006 |
| p53(15−29)pS20[d] | 0.36 | 0.006 |
| p53(15−29)pT18[d] | 3.15 | 0.28 |
| p53(15−29)pS15/pS20[d] | 0.2 | 0.035 |
| p53(15−29)pS15/pT18[d] | 1.317 | 0.3 |
| p53(15−29)pS20/pT18[d] | 2.3 | 0.48 |

[a] Experimental $K_d$ and measurement error are given for each peptide, as reported in the reference specified in the last column. [b] Lai et al.[8] [c] Zondlo et al.[12] [d] Schon et al.[10]

includes only residues 17−29 of p53. Lai et al. were the first to demonstrate the tighter binding of the N-terminal truncated peptide, p53(18−26), having an affinity of 70 nM. Further truncation to p53(19−26) caused a 10-fold reduction in affinity, revealing the critical role of Thr18 in p53 binding to MDM2, and a deletion of the critical Leu26 led to an effectively inactive peptide p53(19−25) (Table 1).

A single-concentration binding assay by Jabbur et al. demonstrated the importance of the Thr18-Asp21 hydrogen-bond network for p53 binding.[9] At the tested concentration, p53(1−52)Thr18Ala, p53(1−52)Thr18Asp, and p53-(1−52)Asp18Ala retained 65%, 47%, and 26% of *wt* activity, respectively, while the non-hydrogen bond disrupting mutation Asp21Asn retained full activity.

A more recent comprehensive study by Schon et al. examined the interaction of MDM2 with a peptide library based on residues 15−29 of p53 using isothermal titration calorimetry (ITC), revealing the effects of peptide length, natural as well as non-natural amino acid substitutions and phosphorylation at Ser/Thr residues.[10] In this study Phe19 and Trp23 were replaced with the non-natural amino acids naphthylalanine (Nal) with a limited loss of activity (∼1.5-

STUDY OF MDM2 BINDING TO p53-ANALOGUES

*J. Chem. Inf. Model., Vol. 49, No. 4, 2009* **867**

fold and ∼2-fold for Phe19 and Trp23, respectively). In the crystal structure, Trp23 makes multiple vdW interactions within the MDM2 binding cleft as well as a hydrogen bond with the carbonyl oxygen of MDM2 Leu54. It is not immediately clear why the loss of a hydrogen bond has such a minor effect on binding. A possible explanation is that it is partially exposed to the solvent. Indole groups are weak hydrogen-bond donors, further weakened with increased polarity of the surroundings.[11] While the weak hydrogen bond is lost, the larger Nal group may gain compensating vdW interactions and may also reduce peptide desolvation penalty due to increased hydrophobicity. This study also demonstrated the tighter binding of shorter peptides (Table 1) and the detrimental effect of the Thr18 phosphorylation. In contrast to the results of Bottger et al.,[5] Leu26 was shown to tolerate a Phe substitution with a mere 2-fold loss in activity. Surprisingly, an identical binding affinity was measured for p53(17−26) and p53(18−26), demonstrating that the highly conserved Glu17 is not important for binding in the context of p53-analogues terminating at Leu26.

A study by Zondlo et al. provided interesting results for several p53 mutations, measured in a fluorescence polarization assay on the background of p53(12−30).[12] In this study, Leu26Ile had no effect on binding, while the Trp23Leu mutation was detrimental, reducing peptide affinity from 229 nM to 45 μM. This study was the first to demonstrate that a single mutation to Pro27 can have a significant positive effect on binding, Pro27Ser improving affinity of p53(12−30) by 100-fold to 4.7 nM. This result implies that the conserved Pro27 may be reducing the inherent affinity of p53 to MDM2, thereby protecting p53 from excessive down regulation by MDM2. p53(12−30)Pro27Ser was examined by CD and NMR and shown to be significantly more helical than *wt* p53(12−30),[12] which improves the peptide's conformational predisposition toward binding. Interestingly, in this study Asp21Ala had almost no effect on binding, in contrast to the results of others.[2,5,9]

It is important to note the effect of phosphorylation on p53 activity. p53 function is regulated by a variety of post-translational modification, the major of which being phosphorylation of Ser/Thr residues by several kinases following cellular stress such as DNA damage.[1,13,14] Phosphorylated Ser15 mediates interaction with the closely related transcriptional coactivating proteins p300 and CBP (CREB Binding Protein) but has little effect on the interactions of p53 with MDM2.[8,10,14,15] This is in agreement with p53 residues Ser15 and Gln16 being disordered in the crystals.[6] Phosphorylation of Ser20 has a pivotal role in regulating the MDM2-mediated turnover of p53 following DNA damage[14] but was also found to have an insignificant effect on p53 binding to MDM2.[10] This is in agreement with crystal structure data showing that Ser20 points out of the binding site, in proximity to p53 residue Lys24, which may gain interaction with the phosphate group. The only phosphorylation disrupting p53 binding to MDM2 is at Thr18.[8,10] It has been argued that the hydrogen-bonding network between Thr18 and Asp21 helps initiate the p53 helix, required for binding MDM2, and that phosphorylation of Thr18 would abolish these interactions, leading to a reduction in binding affinity.[8] In addition, it has been suggested that phosphorylation of Thr18 may cause
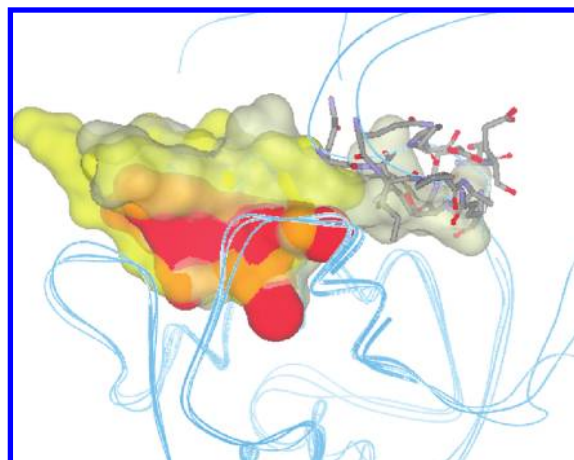


**Figure 2.** The binding-site lid. The 1YCR, 1T4F, and 1RV1 complexes of MDM2 with p53, 9-mer peptide, and small molecule inhibitor, respectively, superimposed with representative NMR conformations of apo-MDM2 from 1Z1M (blue ribbons). In the apo-structure, the proposed lid residues, Gln18-Gln24 (sticks in element color), penetrate into the shallow end of the p53 binding site, occupied by residues 27−29 of the p53 peptide in the 1YCR structure. Both 9-mer peptide (yellow surface) and small molecule inhibitor (red surface) occupy roughly the same space and seemingly are able to coexist with the lid in its "closed" state, while p53(15−29) (gray surface) shows significant overlap with the lid residues and probably pushes it away upon binding. This is in accordance with the results of Showalter et al. showing that nutlin-3 does not interrupt the "closed" state of the lid, in contrast to p53(17−29). This also implies that short peptides, terminating before Pro27, may coexist with closed lid, which may explain their higher affinities as described in the text.

electrostatic repulsion between the modified Thr18 and the proximal Asp21 side chain that could further destabilize the complex.[8]

One of the most intriguing results is the tighter binding of short p53 analogues, terminating at Leu26 (Table 1). The NMR findings of Uhrinova et al. may provide an explanation for the higher affinity of these peptides.[16] This study showed that in the unbound form of MDM2, residues Gln18-Gln24 appear to have some order, invading the shallow end of the p53-binding groove which is occupied by p53 residues 27−29 in the crystal structure of the complex (Figure 2). Especially notable is the position of Ile19, which occupies the same space taken by Pro27 of p53 and may compete with Pro27 for interactions with Tyr100 of MDM2.[16] Gln18-Gln24 are suggested to form a flexible lid over the p53 binding site, which is displaced by p53 upon binding. p53 analogues terminating at Leu26 may possibly coexist with the closed lid, requiring a smaller conformational rearrangement in MDM2 than peptides extending beyond position 26. Uhrinova et al. proposed this theory as an explanation for the tighter binding of short peptides. A recent NMR study by Showalter et al.[17] revealed that the N-terminal lid of MDM2 slowly interconverts between a "closed" state, associated with the p53 binding cleft, and an "open" state which is highly flexible. While apo-MDM2 predominantly populates the "closed" state, binding of p53(17−29) shifts the equilibrium toward the "open" state. In contrast, the binding of nutlin-3, a small molecule inhibitor of p53 binding, does not change the relative prevalence of the two states. Crystal structure data imply that this may also be the case for short peptides, terminating at position 26 or before, as suggested by Uhrinova et al. Figure 2 shows an overlap
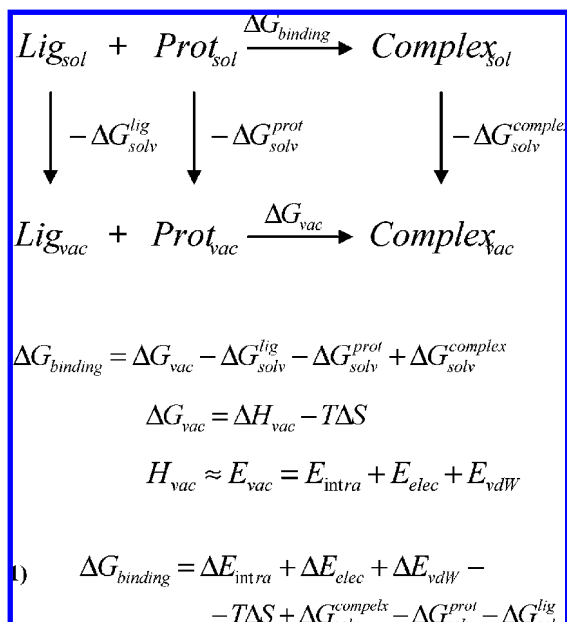
$$Lig_{sol} + Prot_{sol} \xrightarrow{\Delta G_{binding}} Complex_{sol}$$

$$\downarrow -\Delta G^{lig}_{solv} \quad \downarrow -\Delta G^{prot}_{solv} \quad \downarrow -\Delta G^{complex}_{solv}$$

$$Lig_{vac} + Prot_{vac} \xrightarrow{\Delta G_{vac}} Complex_{vac}$$

$$\Delta G_{binding} = \Delta G_{vac} - \Delta G^{lig}_{solv} - \Delta G^{prot}_{solv} + \Delta G^{complex}_{solv}$$

$$\Delta G_{vac} = \Delta H_{vac} - T\Delta S$$

$$H_{vac} \approx E_{vac} = E_{intra} + E_{elec} + E_{vdW}$$

$$(1) \quad \Delta G_{binding} = \Delta E_{intra} + \Delta E_{elec} + \Delta E_{vdW} -$$
$$- T\Delta S + \Delta G^{complex}_{solv} - \Delta G^{prot}_{solv} - \Delta G^{lig}_{solv}$$

**Figure 3.** Thermodynamic cycle used for calculating binding free energies in MM-GB/SA. $\Delta G_{binding}$ is the free-energy of binding in solution; $\Delta G^{lig}_{solv}$, $\Delta G^{prot}_{solv}$, and $\Delta G^{complex}_{solv}$ are the solvation free energies of the ligand, the protein, and the complex, respectively; $\Delta G_{vac}$ is the free energy of binding in vacuum; $E_{intra}$, $E_{elec}$, and $E_{vdW}$ are the force field intramolecular, electrostatic, and vdW energies, respectively. Equation 1 is the final MM-GB/SA equation.

between apo-MDM2 and cocrystal structures of MDM2 in complex with p53(15−29), a 9-mer analogue of p53(18−26), and nutlin-2 (a small molecule inhibitor closely related to nutlin-3[18]). While residues 27−29 of p53(15−29) overlap with the lid residues, it seems that both small molecule and short peptide may coexist with the closed lid.

Interestingly, in the context of short peptides, deletion of Glu17 was shown not to affect binding (Table 1), despite favorable electrostatic interactions with Lys94 and His73 of MDM2 observed in the 1YCR crystal structure. Strangely, the extent to which deletion of both Thr18 and Glu17 affects binding is somewhat controversial. According to Schon et al., the $K_d$ of p53(19−26) is over 5 $\mu$M, 10-fold less potent than p53(15−29) and at least 100-fold less potent than p53(17−26).[10] In contrast, Lai et al. show that p53(19−26) is similar in activity to p53(10−29) and merely 16-fold less potent than p53(17−26)[8] (Table 1).

A better understanding of these complex effects can be achieved by computational techniques, revealing the dynamic behavior of the protein−ligand complexes and the relative contributions of different energetic terms to complex formation. Theoretical tools have been used in the past to investigate the p53-MDM2 interaction.[19−22]

In a pioneering work, Massova and Kollman[19] applied computational alanine scanning based on MM-PB/SA (Molecular Mechanics Poisson−Boltzmann/Surface Area, Figure 3) calculations to study the interaction of MDM2 with p53(16−27) in light of the results of Bottger et al.[5] Although Phe19, Leu22, Trp23, and Leu26 were successfully identified as the key binding determinants, some predictions seem inconsistent with experimental data: Thr18Ala and Asp21Ala were predicted to have no effect on binding, in contrast to mutational and deletion results.[2,5,8−10] The positive effect of the Leu22Tyr mutation was predicted to be due to helix-

stabilizing interactions between Tyr22 and Glu17 contributing favorably to binding despite a disruption of the Trp23 and Phe19 hydrogen bonds. Zhong et al. used the same MM-PB/SA methodology to identify critical residues for binding in both p53 and MDM2, and their results for p53 mutations are similar to those of Massova and Kollman.[19] A more recent paper by Lee et al. addressed the issue of p53 phosphorylation, also using MM-GB/SA.[22] One interesting finding from this study is that phosphorylation at Thr18 does not disrupt the helical conformation of p53 in solution as previously suggested. Local anionicity of MDM2 leading to electrostatic repulsion of the phosphate group was suggested to cause the reduced affinity of pThr18.[22] As expected from experiment, phosphorylation at Ser20 was predicted to have a smaller effect than at Thr18. However, pSer20 and pThr18 were predicted to be 2- and 4-orders of magnitude less active than *wt*, respectively, in disagreement with experimental data (Table 1). In addition, the double phosphopeptide pSer20/Thr18, which has a $K_d$ of 2.3 $\mu$M[10] was predicted to be completely inactive. Recently, Dastidar et al.[23] published an explicit-solvent MM-GB/SA study with interesting results for the Pro27Ser mutant. In solution, this peptide was modeled in an α-helical conformation, in accordance with experimental results.[12] However, in complex with MDM2, the peptide was modeled once as an α-helix and once in *wt* conformation. In both cases, the mutant was found to be more active than *wt*. While the helical conformation was found to have an enthalpic advantage, the *wt* conformation had an entropic advantage. It is not clear which conformation exists in reality. Interestingly, when the mutant was modeled as α-helical in the complex, Tyr100 from MDM2 flipped during the simulation from the 1YCR *trans* conformation to the *gauche(-)* conformation common to all cocrystal structures with short peptides and small molecules (e.g., 1T4F, 1T4E, 1RV1, 2GV2, 2AXI). Together with the compactness of the helical conformation, this may indicate that the Pro27Ser mutant binds in α-helical conformation coexisting with the binding-site lid, which may contribute to its high affinity.

Each of the previous computational studies covered a small portion of the available empirical data described above. The abundance of untreated data and the controversy between experiment and some of the computational results provide motivation for the present work, which attempts to address a diverse set of p53 modifications including mutations to natural as well as non-natural amino acids, regulatory phosphorylations and deletions.

## RESULTS AND DISCUSSION

The following p53-derived peptides were modeled in complex with MDM2 as described in Methods: p53(15−29), p53-(15−29)Thr18Ser, p53(15−29)Phe19Nal, p53(15−29)Leu-22Tyr, p53(15−29)Trp23Nal, p53(15−29)Trp23Leu, p53-(15−29)Leu26Phe, and p53(15−29)Pro27Ser; all combinations of single and double-phosphorylations of p53(15−29) at Ser15, Ser20, and Thr18; p53(17−26), p53(17−26)Phe19Nal, p53(17−26)Phe19MePhe, p53(17−26)Trp23Nal, p53(18−26), and p53(19−26); all p53(15−29) alanine mutants.

As discussed in the Introduction and shown in Table 1, there are inconsistencies in the binding affinities reported for several p53 analogues. Since the majority of the peptides

STUDY OF MDM2 BINDING TO p53-ANALOGUES

*J. Chem. Inf. Model., Vol. 49, No. 4, 2009* **869**

studied here were reported by Schon et al.,[10] we relied on the binding affinities reported by these authors whenever possible.

As described above, most of the previous computational studies of p53-MDM2 binding used classical MM-P(G)B/SA, employing constant pressure MD simulations of a fully hydrated system.[19,20,22,23] These calculations are highly time-consuming (In our hands ~1 CPU day is required for 100 ps of CHARMM simulation on an Intel Xeon E5310 1.60GH with 2GB RAM.) and thus are less suitable for studying large data sets. Therefore, we decided to use GB/SA implicit-solvent simulations, which may be less accurate but are 10-fold faster. Implicit-solvent simulations have been used in the past for free energy prediction within the context of Linear Interaction Energy[24] and Thermodynamic Integration,[25] but we are not aware of previous reports of MM-GB/SA calculations using ensembles generated with continuum solvent MD. Due to the high flexibility of the unbound p53-derived peptides, which may lead to inadequate conformational coverage, we decided to use single-trajectory MM-GB/SA. This method, extracting the conformational ensemble of the unbound protein/ligand from the ensemble of the protein−ligand complex, has been shown to reach better convergence than the multiple trajectory approach relying on independent simulations of the bound and unbound states.[19,22,26] This method neglects the energetic contribution of conformational rearrangements upon binding, and thus inaccuracies may be expected when predicting the relative affinities of peptides with significantly different solution conformations. Calculations were initially performed with CHARMM.[27] However, despite careful optimization of the simulation protocol, stressing the importance of robust temperature control, CHARMM simulations did not yield satisfactory results. Therefore MacroModel[28] Stochastic Dynamics simulations (Methods) were tested as a potential alternative. In our hands, MacroModel was found better suited for this system than CHARMM and was therefore used here. Details of the CHARMM protocol optimization as well as a comparison of the performance of CHARMM and MacroModel are provided in the Supporting Information.

On a side note, we first estimated the applicability of single-conformation MM-GB/SA scoring, successfully used by others for ranking congeneric series of compounds.[29,30] Calculations were performed both with CHARMM[27] and MacroModel[28] (Methods), but no correlation was found between experimental affinities and calculated binding energies.

MM-GB/SA binding energies were first calculated for all p53(15−29) nonphosphorylated and single-phosphorylated derivatives with measured binding affinities from the work of Schon et al.,[10] obtaining a good correlation with experimental $pK_d$ values ($R^2=0.77$, Figure 4a). The following section provides interpretation for the relative affinities of these peptides and subsequently discusses the effect of double-phosphorylations, mutations studied exclusively by Zondlo et al.[12] and Leu22Tyr, for which binding affinity has not been reported. Prediction results are summarized in Table 2. We note that the calculated free energies of binding are an order of magnitude larger than the experimental $\Delta G$ values. This is probably mostly due to the omission of the entropy penalty term (discussed in the Supporting Information). As noted by Gilson and Zhou, the loss in configura-
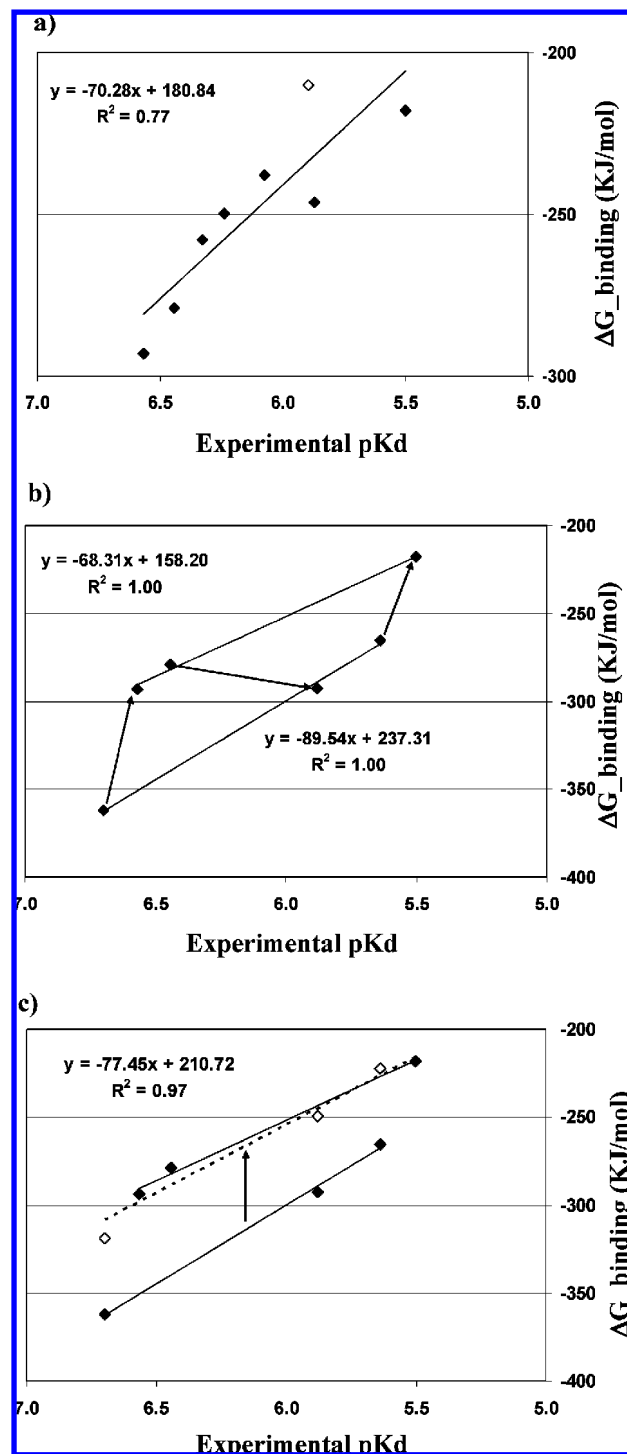


**Figure 4. a)** Correlation between calculated $\Delta G$ and experimental $pK_d$ values for **a)** eight p53(15−29) analogues (first eight in Table 1). Hollow diamond: p53(15−29)Leu26Phe **b)** phosphopeptides. Top regression line: single-phosphopeptides. Bottom regression line: double-phosphopeptides. There is a perfect correlation within each individual series; however, the two regression lines are parallel displaced. **c)**. Displacing the double-phosphopeptide series by a constant value equal to the difference between the averages of the two series (hollow diamonds) results in a near perfect correlation with $R^2=0.97$ (dashed line).

tional entropy cancels most of the binding energy, the actual net binding free energy being a small difference between larger numbers.[26]

p53(15−29)Trp23Nal was predicted to be as active as *wt* p53(15−29). Although the actual predicted affinity is slightly

**870** *J. Chem. Inf. Model., Vol. 49, No. 4, 2009*

KALID AND BEN-TAL

**Table 2.** MacroModel MM-GB/SA Values for p53(15−29) Analogues[a]

| peptide | $\Delta G$ | $\Delta G_{GB}$ | $\Delta G_{SA}$ | $\Delta E_{elec}$ | $\Delta E_{vdW}$ |
|---|---|---|---|---|---|
| P53(15−29) | −249.7 (21.3) | 1,845.2 (82.6) | −21.0 (1.8) | −1,899.0 (100.1) | −175.0 (23.1) |
| p53(15−29)F19Nal | −237.7 (19.9) | 1,878.7 (51.1) | −9.3 (2.0) | −1,926.2 (64.9) | −180.9 (22.2) |
| p53(15−29)W23Nal | −246.3 (24.0) | 1,921.1 (75.7) | −14.7 (2.4) | −1,958.5 (79.9) | −194.2 (26.9) |
| p53(15−29)L26F | −210.0 (34.9) | 1,770.3 (68.6) | −17.3 (1.8) | −1,801.5 (81.0) | −161.4 (28.3) |
| p53(15−29)T18S | −257.7 (19.1) | 1,849.1 (69.8) | −14.4 (2.3) | −1,913.7 (82.6) | −178.7 (22.4) |
| p53(15−29)pS15 | −293.0 (21.3) | 3,050.9 (54.5) | −22.0 (2.0) | −3,156.8 (63.9) | −165.2 (26.7) |
| p53(15−29)pS20 | −279.0 (35.2) | 2,737.2 (75.3) | −18.5 (2.1) | −2,817.5 (86.1) | −180.2 (24.2) |
| p53(15−29)pT18 | −217.9 (15.6) | 2,542.6 (46.1) | −19.8 (2.0) | −2,560.1 (53.5) | −180.7 (21.8) |
| p53(15−29)L22Y | −262.9 (18.2) | 1,886.5 (61.2) | −16.2 (1.8) | −1,919.2 (70.5) | −214.0 (21.8) |
| p53(15−29)W23L | −178.0 (17.3) | 1,639.3 (57.3) | −18.8 (1.6) | −1,651.6 (61.1) | −146.9 (19.7) |
| p53(15−29)D21A | −234.6 (21.3) | 1,337.6 (60.8) | −19.3 (1.7) | −1,357.0 (75.8) | −195.9 (22.3) |
| p53(15−29)pT18/S20 | −265.1 (20.8) | 3,550.1 (83.7) | −19.3 (1.4) | −3,587.4 (91.1) | −208.5 (17.4) |
| p53(15−29)pS15/T18 | −292.5 (22.5) | 3,299.2 (71.9) | −20.3 (2.0) | −3,366.0 (84.8) | −205.5 (21.9) |
| p53(15−29)pS15/pS20 | −361.8 (19.2) | 3,952.9 (65.5) | −14.8 (2.1) | −4,125.1 (75.4) | −174.8 (22.8) |
| p53(15−29)E17A | −153.6 (17.3) | 1,062.5 (66.0) | −15.5 (2.2) | −1,026.2 (69.5) | −174.4 (21.0) |
| p53(15−29)T18A | −221.3 (19.2) | 1,869.4 (62.0) | −17.6 (1.9) | −1,904.0 (76.0) | −169.2 (20.6) |
| p53(15−29)F19A | −218.1 (22.0) | 1,764.4 (83.4) | −16.6 (1.7) | −1,803.3 (100.7) | −162.5 (23.4) |
| p53(15−29)L22A | −269.9 (20.3) | 1,941.5 (82.9) | −17.0 (1.9) | −2,017.3 (100.0) | −177.1 (21.8) |
| p53(15−29)W23A | −171.8 (21.0) | 1,712.5 (83.4) | −17.1 (1.7) | −1,741.9 (102.6) | −125.4 (23.2) |
| p53(15−29)K24A | −265.5 (30.0) | 2,193.2 (64.9) | −16.7 (1.7) | −2,266.8 (91.3) | −175.1 (24.7) |
| p53(15−29)L25A | −216.5 (19.8) | 1,863.3 (55.4) | −19.2 (2.0) | −1,902.1 (67.9) | −158.5 (20.7) |
| p53(15−29)L26A | −210.6 (20.8) | 1,897.3 (82.6) | −15.7 (1.7) | −1,942.9 (100.0) | −149.3 (21.9) |
| p53(15−29)P27S *wt-conf* | −245.4 (117.6) | 1,568.1 (99.3) | −15.8 (4.4) | −1,573.2 (135.3) | −224.6 (84.9) |
| p53(15−29)P27S *helical* | −160.1 (21.3) | 1,413.6 (153.7) | −13.6 (2.3) | −1,395.3 (154.7) | −164.8 (34.1) |
| p53(15−29)E28A | −212.2 (30.4) | 1,146.4 (183.3) | −20.0 (2.1) | −1,132.2 (207.0) | −206.4 (16.7) |
| p53(15−29)N29A | −195.8 (19.9) | 1,853.8 (101.8) | −16.6 (2.1) | −1,881.5 (115.3) | −151.4 (18.9) |

[a] A breakdown of the calculated binding energy ($\Delta G$) into individual components is given for each peptide. $\Delta G_{GB}$, $\Delta G_{SA}$: electrostatic and nonpolar components of the free energy of solvation, respectively. $\Delta E_{elec}$, $\Delta E_{vdW}$: electrostatic and vdW components of the binding enthalpy (See Figure 3 for details). Standard deviation is given in parentheses. p53(15−29)Pro27Ser was modeled in both *wt* and helical conformation.

lower, $\Delta G$ distributions were compared using student's *t* test and were found to be indistinguishable ($P > 0.1$). While the reported $K_d$ for this peptide is 1.35 $\mu$M, the measurement error is 0.4 $\mu$M, the largest among the peptides tested by Schon et al.[10] The correlation obtained with MM-GB/SA may be further improved if the lower bound value is used instead of the reported average. Interestingly, in addition to gaining vdW contacts due to the larger Nal group, this peptide also seems to gain electrostatic interactions despite the loss of the Trp23 hydrogen bond. This may indicate that p53(15−29) is capable of compensating for the loss of a hydrogen bond by gaining additional interactions, in contrast to its shorter analogue p53(17−26), discussed below.

p53(15−29)Phe19Nal was predicted to be slightly less active than *wt*, as expected from experiment.

Thr18Ser was predicted to be slightly more active than *wt*, in accordance with experimental results. This seems to be due to improved electrostatic and vdW interactions. During the MM-GB/SA MD simulations, Thr18 did not maintain its hydrogen bond with the Asp21 side chain. In contrast, Ser18 maintained a stable hydrogen bond with the Asp21 side chain and also gained additional transient hydrogen bonds with Ser20 and the Asp21 backbone.

MM-GB/SA predicted Leu26Phe to be less active than expected. In this case, the deviation from the regression line is larger than for the other variants included in the correlation (Figure 4a). This problem was addressed by inspecting the distribution of individual MM-GB/SA $\Delta G$ values calculated at each sampled MD frame; the final MM-GB/SA energy is an average of these values. Surprisingly, the distribution of $\Delta G$ values for Leu26Phe was far from a normal distribution (Figure 6), which may indicate that the calculation has not converged. Indeed, rmsd analysis reveals that the Leu26Phe
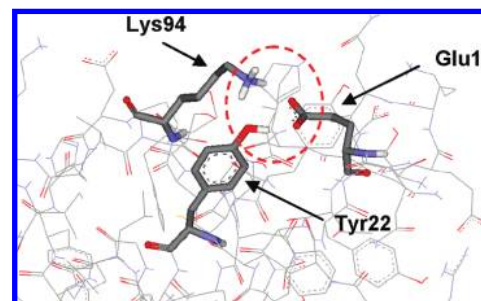


**Figure 5.** Interactions between Tyr22, Glu17, and MDM2 Lys94 observed during MD simulations within the time frame used for MM-GB/SA sampling. A hydrogen bond network is formed between Try22 phenol hydroxyl, Glu17, and MDM2 Lys94. In addition, the Tyr22 phenyl ring packs against the Lys94 side chain, gaining additional vdW interactions compared to the *wt* Leu22.

simulation was significantly less stable than *wt*. It is possible that the initial conformation used for modeling this mutant in complex with MDM2 is not optimal, but this issue was not pursued further. Exclusion of this mutant from the correlation increases $R^2$ from 0.77 to 0.84.

Interesting results were obtained for the three single-phosphorylated peptides. The binding affinities predicted for these peptides correlate well with experimental affinities providing a good rank ordering both within this group ($R^2$=1, Figure 4b) and relative to nonphosphorylated peptides (Figure 4a). This supports the credibility of the current computational interpretation which differs significantly than that of Lee et al., described above.[22] According to the current MM-GB/SA calculation, phosphorylations modulate p53 affinity through interplay between two opposing factors: favorable electrostatic interactions and desolvation. For all three peptides there is a significant electrostatic gain. It is largest
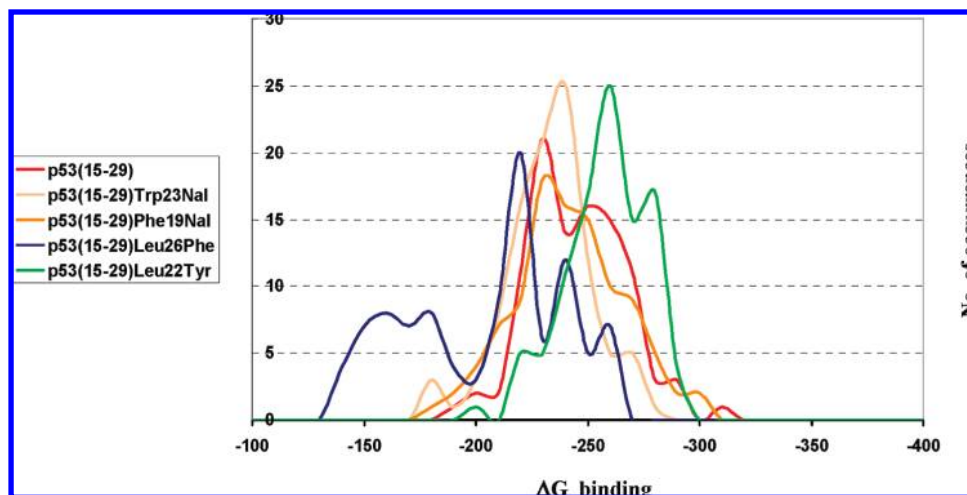
STUDY OF MDM2 BINDING TO p53-ANALOGUES

*J. Chem. Inf. Model., Vol. 49, No. 4, 2009* **871**

**Figure 6.** Distribution of calculated $\Delta G$ values over the ensemble of conformations that were sampled during the MD simulations. The reported $\Delta G$ is the average of these values. $\Delta G$ distribution is expected to be roughly normal, which is indeed the case for all the tested peptides (five representative distributions are shown). However, this is not the case for the Ley26Phe peptide (dark blue). This may indicate that the calculation for this mutation has not converged and that the system requires more time to conformationally adjust to the mutation.

for pSer15, due to favorable interactions with MDM2 residue Lys94 and the p53 N-terminus (Figure 7a). A smaller gain is predicted for pSer20 interacting with p53 residue Lys24 (Figure 7b). The smallest increase in $\Delta E_{elec}$ is predicted for pThr18 which during simulation becomes caged within a network of hydrogen bonds with p53 backbone amides and Gln16 (Figure 7c). These interactions are counterbalanced by a significant increase in the polar desolvation term $\Delta G_{GB}$, providing the correct rank ordering. There is no evidence of electrostatic repulsion due to the presence of an anionic patch as suggested by Lee et al.[22]

It has been suggested previously that the lower activity of pThr18 is due to reduced p53 helicity following the loss of the Thr18-Asp21 hydrogen bond.[12] This idea challenges the validity of our MM-GB/SA interpretation, which provides a good correlation while ignoring differences in the unbound conformational ensemble. Therefore, we decided to perform complementary MD simulations of the unbound *wt* and phosphorylated peptides (Methods) to address the effect of Thr18 phosphorylation on p53 helicity. In accordance with the results of Lee et al.[22] no change in helical stability was observed upon phosphorylation (Figure 8), lending further credibility to our MM-GB/SA results.

The results for double-phosphorylated peptides are also very exciting. As for the single-phosphorylated peptides, the correlation between calculated free energies and experimental binding affinities within this group was very good ($R^2=1$, Figure 4b), $\Delta G$ being governed by a balance between favorable electrostatics and desolvation. MM-GB/SA binding energies of the double-phosphopeptides seem to deviate by a constant factor from those of the single-phosphopeptides, as apparent from the two parallel displaced regression lines (Figure 4b). Adding a constant factor to the MM-GB/SA energies of the double-phosphopeptides, equal to the difference between group averages, leads to a perfectly correlated set of binding energies (Figure 4c). Displacement by a constant factor may indicate an overestimation of either $\Delta E_{elec}$ or $\Delta G_{GB}$ due to the presence of excess charge (double-phosphopeptides have a formal charge of $-6$ compared with $-4$ for the single-phosphopeptides and a maximum of $-2$

for the rest of the peptides analyzed). This may be due to limitations of force field, solvation model, or cutoff value used for calculating the electrostatic interactions (Methods) and should be investigated further. Surprisingly, for this set of peptides, implicit-solvent MM-GB/SA appears to be more accurate than the explicit-solvent ns-scale MM-GB/SA of Lee et al., which obtained a positive $\Delta G$ value for pThr18/pSer20.[22]

In contrast to the mutations discussed above, Trp23Leu, Asp21Ala, and Pro27Ser have been tested exclusively by Zondlo et al.,[12] on the background of p53(12−30). This p53 segment was reported to have an affinity of 0.229 $\mu$M, compared with 0.575 $\mu$M measured for p53(15−29) by Schon et al.[10] (Table 1). Due to the lack of a common reference frame, these peptides were excluded from the correlation described above.

As expected, the Trp23Leu mutation was predicted to be detrimental to binding due to a significant loss of protein−ligand interactions.

Asp21Ala was predicted to be less potent than *wt* due to concurrent loss in electrostatic energy and improvement in the solvation energy of the complex. The calculated $\Delta\Delta G$ translates to a ∼2-fold activity loss relative to *wt* (Methods), in contrast to a small activity gain reported by Zondlo et al.[12] However, an activity loss is in agreement with other experimental studies.[2,5,9] Based on crystal structure data, the Asp21-Thr18 hydrogen bond has been suggested to be important for p53 helix initiation.[6] To test this hypothesis, simulations of the unbound mutant peptide in solution were performed, as for pThr18. In accordance with the suggestion above, the mutant peptide was found to be significantly less helical in solution than *wt* (Figure 8). This indicates that Asp21 is indeed important for p53 binding, contrary to the results of Zondlo et al., and that p53(15−29)Asp21Ala may be significantly less active that predicted by MM-GB/SA.

Pro27Ser, found by Zondlo et al. to be significantly more $\alpha$-helical in solution than *wt* p53,[12] was modeled twice: once in *wt* conformation and once in helical conformation (as in ref 23). In both cases the prediction did not match the experimental data. This was further addressed following the
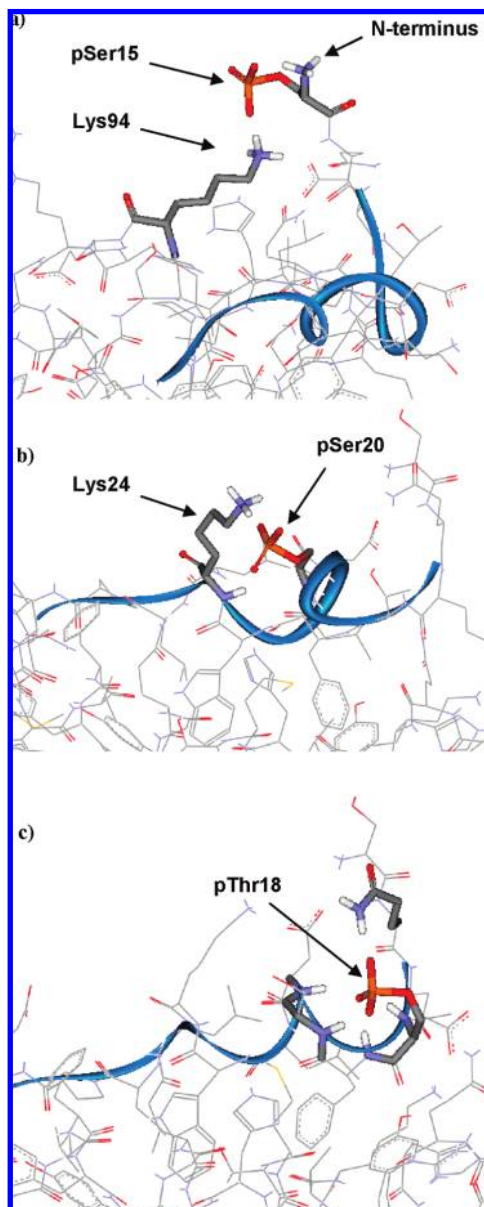
**Figure 7.** Interactions of phosphate groups observed during the MD simulation within the time frame used for MM-GB/SA sampling. **a)** pS15 is involved in two salt bridges, with the peptide N-terminus and with MDM2's Lys94. **b)** pS20 is engaged in a salt bridge with p53 Lys24. **c)** pT18 is enclosed in a cage of five hydrogen bonds with p53 backbone amides and p53 Gln16 side chain.
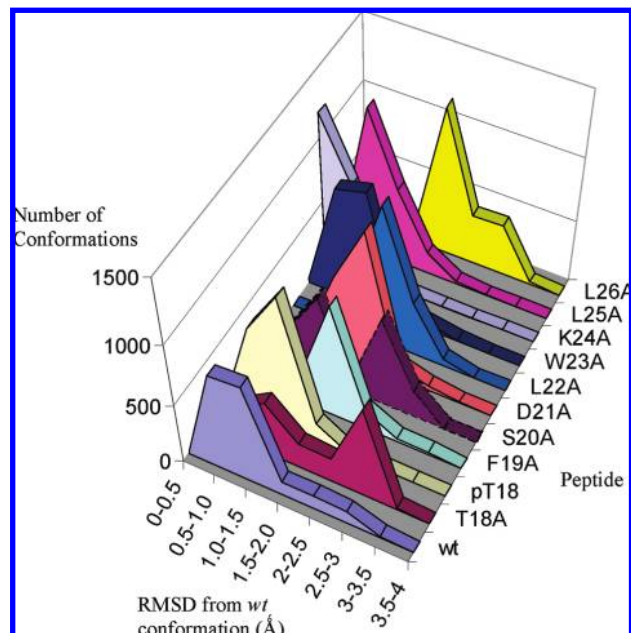


**Figure 8.** Stability of bound conformations in solution. Stability of the p53 helical conformation in solution calculated for *wt* and mutant peptides over a 100 ns MD simulation. Stability is represented as the distribution of p53(19−23) backbone rmsd relative to the *wt* bound conformation. Significant disturbance is seen upon disruption of the Thr18-Asp21-Ser20 hydrogen-bond network and upon removal of either Phe19 or Leu26 which pack against Trp23 as well as Leu22. The strongest helix disturbing mutations are Leu26Ala and Thr18Ala. For each p53(15−29) mutant (Y-axis), the number of peptide conformations (Z-axis) is plotted against ranges of rms deviation from *wt* (Methods).

modeling of p53 analogues terminating at Leu26 and is discussed below.

Finally, Leu22Tyr was predicted by MM-GB/SA to have a stronger effect on binding than either of the Nal mutations, and the predicted affinity correlates well with the experimental 2-fold improvement over *wt* reported by Bottger et al.[5] Specifically, by translating MM-GB/SA energies into predicted $pK_d$ values (Methods) a factor of 1.5 over *wt* affinity is obtained. Relative to Leu22, Tyr22 shows increased vdW and electrostatic interactions. The Tyr22 phenol hydroxyl hydrogen bonds to Glu17 and MDM2 Lys94, and its phenyl ring stacks against the alkyl side chain of Lys94 (Figure 5), gaining additional vdW interactions compared to the *wt* Leu22. This positive contribution to binding is attenuated by increased $\Delta G_{GB}$. The lack of interaction with MDM2 residue His73 suggests that the aromatic preference

may not be as relevant for *wt* p53 as it is for the peptides of Bottger et al. which lack Glu17, as proposed in the Introduction. In contrast to the results of Massova et al.,[19] the present calculation did not find a destabilizing effect on p53 hydrogen bonds nor an increased conformational strain in the complex.

Subsequently, p53 residues 17−29 were consecutively mutated to alanine. Experimental affinities have not been reported for these mutants, except for Asp21Ala discussed above. To facilitate easier comparison between predicted affinities, MM-GB/SA energies were translated into $pK_d$ values (Methods). Helical stability was also assessed for each of the mutants (Methods).

p53(15−29)Thr18Ala was found to be significantly less potent than *wt* p53.[2,9] In our calculation, it is predicted to have reduced affinity of ∼2 μM, mostly due to a larger desolvation penalty than *wt* (Table 2). In addition, its helical stability in solution was strongly diminished (Figure 8), suggesting further reduced binding affinity. This result is in agreement with the helix stabilizing role previously suggested for Thr18.[6] Throughout the simulation of the unbound *wt* peptide, a stable hydrogen bond was observed between the side chains of Thr18 and Asp17, and an additional, transient, hydrogen bond was found between Thr18 and Ser20. Interestingly, during the MD simulation of the *wt* complex, these hydrogen bonds were mostly lost. This result may indicate that the major role of the Thr18-Asp21 hydrogen-bond network is to stabilize the helical conformation in solution prior to binding.

Phe19Ala was predicted to be less active than *wt* due to a loss in $\Delta E_{vdW}$ and $\Delta E_{elec}$, compensated for, in part, by a

STUDY OF MDM2 BINDING TO p53-ANALOGUES

*J. Chem. Inf. Model., Vol. 49, No. 4, 2009* **873**

reduction in $\Delta G_{GB}$. However, the effect is not detrimental as expected from experiment (Bottger et al.[5] describe a complete loss of activity, results not shown). In the p53 bound conformation, Phe19 packs against Trp23 and may stabilize the p53 amphipathic helix, which is required for binding. Potential destabilization by Phe19Ala may be the source for the reported loss of activity. Indeed, Phe19Ala was found to be significantly less helical than *wt* p53 (Figure 8).

The effect of the Ser20Ala mutation could not be predicted due to rapid ligand drifting during MD, leading to a complete loss of the Trp23 and Leu26 anchoring interactions. The reasons for this conformational instability, which were not seen in the other simulations, are unclear at this point.

The Leu22Ala mutation was shown by Picksley et al. to be detrimental to the binding of p53(16−25).[2] In addition, Bottger et al. demonstrated a significant loss of activity for the 12-mer following this mutation.[5] In contrast, MM-GB/SA predicted a slightly improved affinity, mostly due to an increase in the electrostatic component. While MM-GB/SA failed to perceive the effect of this mutation, Leu22Ala was found detrimental to peptide helicity (Figure 8), in accordance with a role in helix formation proposed by others.[31]

The Trp23Ala mutant was predicted to be detrimental due to reduced $\Delta E_{elec}$ and $\Delta E_{vdW}$, in accordance with experimental results (Table 2). Interestingly, this mutation did not lead to helical instability (Figure 8).

No loss of activity was predicted for the Lys24Ala mutant, in accordance with the Bottger results, revealing a wide tolerance at this position.[5]

Leu25Ala was predicted to reduce binding ∼5-fold, mostly due to reduced vdW interactions and increased desolvation penalty, contrary to the results of Massova et al.[19] Interestingly, the temperature factor of the Leu25 side chain in 1YCR is identical to that of the anchoring residue Leu26, suggesting a role in binding. While Bottger et al. demonstrated a wide tolerance at position 25 of the 12-mer,[5] the relevance of this result to *wt* p53 is not clear since the amino-acid sequence of the 12-mer is adapted for a glycine at this position.

Leu26Ala was predicted to reduce peptide affinity to ∼3 $\mu$M, mostly due to a higher $\Delta E_{vdW}$. As for Phe19, the effect predicted by MM-GB/SA was not as detrimental as suggested by Bottger et al.[5] However, Leu26 was also found critical for helical stability (Figure 8) which may bridge the gap.

Glu17Ala, Glu28Ala, and Asn29Ala were all found to be less active than *wt*. However, these results are probably unreliable. Despite the seemingly favorable interactions observed in 1YCR, Glu28 and Asn29 are only partially resolved in the crystal,[6] and Glu17 has B-factor values as high as those of the former two, indicating a weak contribution to binding of all three residues. Our simulations probably overestimate their contribution.

Following the analysis of p53(15−29) analogues, we addressed the binding of p53 analogues terminating at Leu26 as well as peptidomimetic inhibitors of the p53-MDM2 interaction. The set of peptidomimetics, added to test the applicability of the current MM-GB/SA protocol to drug-design, constituted four helical 8-mer mimetics reported by Garcia-Echeverria et al.[32] (compounds 3, 4, 5, and 8 from that paper) and five beta-hairpins reported by Fasan et al.[33] (compounds 62, 64, 67, 77a, and 78a from that paper).
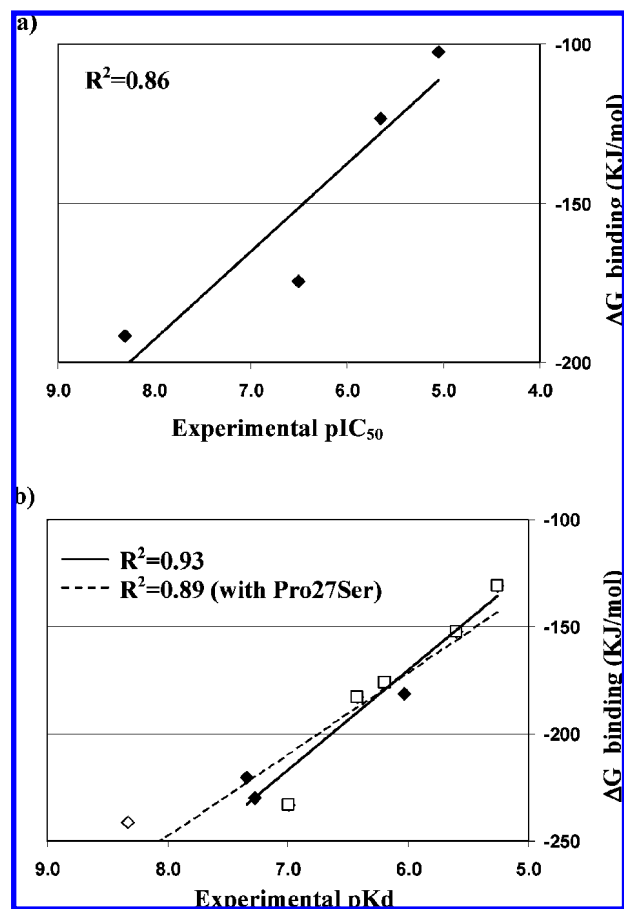


**Figure 9.** Correlation between calculated $\Delta G$ and experimental $pK_d$ values for the short peptides and peptidomimetics. **a)** Correlation obtained for 8-mer peptidomimetics. **b)** Correlation obtained for beta-hairpin peptidomimetics in combination with p53(17−26) analogues. Hollow squares: beta-hairpin mimetics. Hollow diamond: p53(15−29)Pro27Ser in helical conformation.

Compounds from both papers were selected to span a range of activities (Methods).

Unexpectedly, when the peptides and peptidomimetics were modeled in complex with the structure of MDM2 from 1YCR, no correlation was observed between calculated and experimental affinities. However, good correlations were obtained upon remodeling the protein−ligand complexes using the structure of MDM2 from 1T4F ($R^2$=0.86 for 8-mer mimetics, Figure 9a; $R^2$=0.93 for the beta-hairpins; $R^2$=0.89 for the beta-hairpins combined with peptides terminating at Leu26, Figure 9b). The transition from 1YCR to 1T4F is further discussed in the Supporting Information. Interestingly, the short p53 analogues, 8-mers, and beta-hairpins occupy a similar portion of the MDM2 binding site, all terminating at a position equivalent to Leu26. Thus, 1T4F may be a better template than 1YCR for assessing the binding of peptides terminating at Leu26 and compounds of similar size. As discussed in the Supporting Information, the reasons for this remain unclear at this point.

The significant correlations obtained for peptidomimetics alone and in combination with p53 analogues suggest that implicit-solvent MM-GB/SA may support the design of diverse peptidomimetic inhibitors of the p53-MDM2 interaction. While application to small molecule inhibitors is outside the scope of this work, there is no reason for the present methodology not to be applicable in that case as well.

**Table 3.** MacroModel MM-GB/SA Values for Short p53 Analogues[a]

| peptide | $\Delta G$ | $\Delta G_{GB}$ | $\Delta G_{SA}$ | $\Delta E_{elec}$ | $\Delta E_{vdW}$ |
|---|---|---|---|---|---|
| p53(17−26) | −112.2 (17.7) | 932.3 (56.5) | −12.2 (1.9) | −908.6 (66.7) | −123.8 (20.0) |
| p53(17−26)F19Nal | −122.1 (14.0) | 994.8 (37.8) | −9.0 (1.7) | −969.8 (57.8) | −138.1 (17.5) |
| p53(17−26)W23Nal | −133.7 (12.2) | 1,094.9 (44.1) | −7.6 (1.6) | −1,096.2 (50.9) | −124.7 (18.5) |
| p53(17−26)F19MePhe | −127.2 (15.3) | 1,004.5 (34.2) | −10.0 (2.4) | −1,031.3 (45.6) | −90.5 (16.4) |
| p53(15−29)Pro27Ser-helical | −241.5 (15.9) | 1,692.0 (74.8) | −18.1 (2.1) | −1,750.3 (80.7) | −165.1 (20.0) |

[a] A breakdown of the calculated binding energy ($\Delta G$) into individual components is given for each peptide. $\Delta G_{GB}$, $\Delta G_{SA}$: electrostatic and nonpolar components of the free energy of solvation, respectively. $\Delta E_{elec}$, $\Delta E_{vdW}$: electrostatic and vdW components of the binding enthalpy (See Figure 3 for details). Standard deviation is given in parentheses. p53(15−29)Pro27Ser was modeled in a helical conformation.

The MM-GB/SA results for p53 analogues obtained with 1T4F-based MM-GB/SA are summarized in Table 3. An interesting result was obtained for p53(17−26)Trp23Nal. The experimental activity loss associated with the Trp23Nal mutation is much more pronounced for p53(17−26) than for p53(15−29) (Table 1). Correspondingly, our calculations showed a much greater reduction in $\Delta E_{elec}$ in this case, suggesting that the Trp23 hydrogen bond is more critical for shorter peptides. This may indicate that longer peptides are able to compensate for the loss of this specific interaction by gaining others.

As discussed in the Introduction, p53(15−29)Pro27Ser adopts a helical conformation in solution and was suggested to be helical when bound to MDM2. In the helical conformation, this peptide is similar in size to p53 analogues terminating at Leu26 (size similarity was evaluated by superimposing the mutant peptide in helical conformation onto p53(17−26) in *wt* conformation). Therefore, 1T4F-based MM-GB/SA was tested as an alternative to the 1YCR-based predictions discussed above, which were unsuccessful. Subsequent addition of p53(15−29)Pro27Ser to the set of short p53 analogues and beta-hairpin mimetics maintained the correlation quality ($R^2$=0.89, Figure 9b). This result indicates that p53(15−29)Pro27Ser may bind MDM2 similarly to peptides terminating at Leu26, possibly without displacing the binding-site lid, which may contribute to its high affinity. This result is in agreement with the simulations of Dastidar et al.,[23] showing that p53(15−29)Pro27Ser causes Tyr100 in MDM2 to shift into a 1T4F-like conformation.

## CONCLUSIONS

Implicit solvent MM-GB/SA was successfully used to predict the relative binding affinities of p53 analogues to MDM2, including natural as well as non-natural amino-acid substitutions, regulatory phosphorylations, and peptide truncations. MM-GB/SA energy terms were used in conjunction with structural data generated by MD to provide interpretation of experimental results.

Several conclusions can be drawn within the accuracy limits imposed by the absence of amino- and carboxy-termini of MDM2 and the implicit solvent model: **1)** The hydrogen bond between Thr18 and Asp17 is probably important for stabilizing the helicity of p53 in solution, in preparation for binding. Upon binding, the peptide conformation is stabilized by MDM2, and the hydrogen bond is lost. This was revealed by a combination of MM-GB/SA and simulations of unbound *wt* and mutant peptides. **2)** Phe19, Leu22, and Leu26 stabilize the helical conformation of p53 in solution. **3)** Phosphorylation at different positions may regulate p53 MDM2 interaction through a balance between favorable electrostatic

interactions and desolvation penalty. **4)** The Trp23 hydrogen bond seems more critical for the binding affinity of short peptides than for long peptides, potentially due to compensating interactions in the long peptides.

From the computational aspect: **5)** Implicit solvent MM-GB/SA, which is at least 10-fold more efficient than explicit solvent free-energy prediction methods, is applicable to the analysis of protein−protein interactions. One limitation of the method is that protein−protein interactions take place at shallow, relatively solvent exposed binding sites, and the absence of water molecules may lead to greater structural drifts during molecular-dynamics. This may limit the length of the molecular-dynamics simulations and therefore the extent of conformational sampling, potentially effecting prediction accuracy. **6)** Implicit solvent MM-GB/SA may also be applicable as a predictive tool in the design of protein−protein interaction inhibitors. This was exemplified through correlations obtained for two sets of peptidomimetic inhibitors, both individually and in combination with p53 derivatives. **7)** The present results indicate that in the case of shallow solvent-exposed relatively hydrophobic binding sites which pose a challenge for implicit solvent simulations, MacroModel Stochastic Dynamics with GB/SA and OPLS-2005 may perform better than CHARMM Nose-Hoover dynamics with GB/SW and the CHARMM Momany and Rone force field.

## METHODS

**Modeling Protein−ligand Complexes.** 1YCR-based protein−ligand complexes were generated by direct modification of the MDM2-p53(17−29) cocrystal structure using the Schrodinger Maestro Build module.[34] Ser15 and Gln16, missing from the crystal structure, were added to all relevant peptides in extended conformation. 1T4F-based complexes were generated by superimposing peptides from 1YCR-based complexes onto the 9-mer ligand in 1T4F. The p53(15−29)Pro27Ser mutant was modeled in both *wt* and helical conformation. The helical conformation was generated from *wt* by imposing a helical structure on the p53(24−29) residues using the Accelrys Discovery Studio 2.0 Protein Modeling tool.[35] Residues 24−29 were selected to maximize the overlap between *wt* and helical conformations. Peptidomimetics compounds 3, 4, 5, and 8 from the Garcia-Echeverria et al. paper[32] were modeled based on the crystal structure of compound 8 with MDM2 (pdb code 2GV2[36]). In the 2GV2 crystal, the peptide lacks the ACE and NH2 termini described in the Garcia-Echeverria paper. Thus, termini were added in Maestro.[34] Beta-hairpin compounds 62, 64, 67, 77a, and 78a from Fasan et al.[33] were modeled based on the crystal

STUDY OF MDM2 BINDING TO p53-ANALOGUES

*J. Chem. Inf. Model.,* Vol. 49, No. 4, 2009 **875**

structure of compound 78a with MDM2 (2AXI[33]). These compounds were chosen to span a range of activities.

Complexes were prepared for simulation with the Schrodinger protein-preparation tool.[34] Following the addition of hydrogen atoms, protein-preparation optimizes the orientation of hydroxyl and sulfhydryl groups, the protonation and tautomeric states of His side chains, and the "flip" state of Asn, Gln, and His side chains around their outermost Chi angle. Then, a series of short restrained minimizations is performed, optimizing the modified structure while keeping it as close as possible to the crystal structure coordinates. The first minimization iteration reorients side-chain hydroxyls and sulfhydryls by tightly tethering all non-hydrogen atoms with a force constant of 10 kcal/mol·Å² and minimizing with torsion interactions turned off. The following minimizations use a restored torsion potential and progressively weaker position restraints on the non-hydrogen atoms, using force constants of 3, 1, 0.3, and 0.1 kcal/ mol·Å². Each minimization terminates at 100 steps, when the potential energy gradient reaches 0.05 kcal/mol·Å or when the heavy-atom rmsd deviation from the initial coordinates reaches 0.3 Å. Conjugate-gradients minimization is performed using *Impact*[37] with the OPLS_2001 force-field and a distance dependent dielectric of 4.

**Activity Data for Peptidomimetics.** Comparing activities of compounds studied in different types of assays and/or assay conditions requires $K_d$ rather than IC$_{50}$. $K_d$ values were obtained for the beta-hairpins by converting the reported IC$_{50}$ values using the Cheng-Prussof equation.[38] The data required for conversion were not available for the 8-mer compounds. Thus, 8-mers were analyzed separately, while the beta-hairpins were analyzed both independently and in combination with the p53(17−26) analogues.

**MacroModel Single-Point MM-GB/SA.** Complexes were typed with the OPLS-2005 force-field. Solvent effects were modeled using a GB/SA implicit solvent model. Structures were minimized using Truncated-Newton minimization terminating after 2000 steps or after reaching a gradient of 0.01 kcal/mol. Following minimization, MM-GB/SA was calculated as $\Delta G = G_{complex} - G_{ligand} - G_{protein}$ using a set of perl and MacroModel python scripts.

**CHARMM Single-Point MM-GB/SA.** Complexes prepared using the procedure described above were typed using the CHARMM Momany-Rone force-field.[35] Solvent effects were modeled with the GB/SW implicit-solvent model. Structures were energy minimized using the Steepest-Descent algorithm followed by Adopted-Basis Newton−Raphson, both terminating after 2000 steps or after reaching a gradient of 0.01 kcal/mol. Following minimization, protein and ligand structures were extracted from the complex, and MM-GB/SA was calculated as $\Delta G = G_{complex} - G_{ligand} - G_{protein}$ using a set of perl and CHARMM scripts.

**MacroModel Implicit Solvent MM-GB/SA.** Complexes were typed with the OPLS-2005 force-field. Solvent effects were modeled using a GB/SA implicit solvent model. Structures were minimized using Truncated-Newton minimization terminating after 2000 steps or after reaching a gradient of 0.01 kcal/mol. Following minimization, Stochastic Dynamics was performed with the following protocol: Gradual heatup from 100 K to 300 K over a period of 20 ps; equilibration + production over a period of 3 ns at constant temperature. All bonds to hydrogen atoms were

constrained using the SHAKE algorithm allowing a time step of 1.5 fs. Coordinates were saved at 2 ps intervals (also see discussion in the Supporting Information).

**MM-GB/SA calculation:** Single-trajectory MM-GB/SA was performed due to the high flexibility of the unbound 15-mer which may lead to inadequate conformational coverage. This method, in which the conformational ensembles of the unbound protein and the free ligand are extracted from the ensemble of the protein−ligand complex, has been shown to reach better convergence than the multiple trajectory approach.[19,22,26] MM-GB/SA energy terms (see Figure 3) were calculated from 100 snapshots sampled between 200 ps and 400 ps of the simulation (see the Supporting Information for details) using a combination of perl and MacroModel python scripts.

**Translating MM-GB/SA Energies to p$K_d$ Values.** MM-GB/SA predictions for eight p53(15−29) analogues correlated well with experimental affinities (R²=0.77). The regression line describing the correlation has the following equation: MM-GB/SA = −70.28*p$K_d$ + 180.84. This equation can be reorganized to describe p$K_d$ as a function of MM-GB/SA energy. The new equation reproduces p$K_d$ values for these eight compounds with an average unsigned error of 0.16 log units. When predicting the affinity of peptides without experimentally measured affinities, MM-GB/SA energies can be translated into estimated p$K_d$ values using the new equation, and the prediction error can be roughly estimated using the calculated average error.

**MacroModel Simulations for Assessing Conformational Stability.** Peptides were typed with the OPLS-2005 force-field. Solvent effects were modeled using a GB/SA implicit solvent model. Nonbonded interactions were treated with a cutoff of 8 Å for vdW interactions and 20 Å for electrostatics, as required for MacroModel[28] GB/SA simulations according to the program manual. Structures were minimized using Truncated-Newton minimization terminating after 2000 steps or after reaching a gradient of 0.01 kcal/mol. The following MD cascade was then carried out: Gradual heatup from 100 K to 300 K over a period of 20 ps; equilibration + production over a period of 100 ns at constant temperature. All bonds to hydrogen atoms were constrained using the SHAKE algorithm allowing a time step of 1.5 fs, and Stochastic Dynamics was used for temperature control. Coordinates were saved at 50 ps intervals. In the 1YCR cocrystal structure, p53 residues 19−23 are in helical conformation. Therefore, helical stability was estimated by superimposing all MD snapshots onto the initial structure using the backbone of p53(19−23) for calculating the transformation matrix and for deriving the rms deviations.

**Abbreviations**: MM-GB/SA, molecular-mechanics generalized born/surface area; MD, molecular dynamics; MDM2: mouse double-minute 2.

**Note Added after ASAP Publication.** This article was released ASAP on March 26, 2009 without the Acknowledgment. The correct version was posted on April 3, 2009.

**876** *J. Chem. Inf. Model., Vol. 49, No. 4, 2009*

KALID AND BEN-TAL

**Supporting Information Available:** Detailed description of the optimization stages leading to the final MM-GB/SA simulation protocol, including a critical evaluation of simulation credibility, selection of a proper time window for MM-GB/SA, and a comparison between the performance of CHARMM and MacroModel, and the process leading to the selection of 1T4F as a template for modeling short peptides and peptidomimetics. This material is available free of charge via the Internet at http://pubs.acs.org.

## REFERENCES AND NOTES

(1) Woods, D. B.; Vousden, K. H. Regulation of p53 function. *Exp. Cell Res.* **2001**, *264*, 56–66.

(2) Picksley, S. M.; Vojtesek, B.; Sparks, A.; Lane, D. P. Immunochemical analysis of the interaction of p53 with MDM2; - fine mapping of the MDM2 binding site on p53 using synthetic peptides. *Oncogene* **1994**, *9*, 2523–2529.

(3) Lin, J.; Chen, J.; Elenbaas, B.; Levine, A. J. Several hydrophobic amino acids in the p53 amino-terminal domain are required for transcriptional activation, binding to mdm-2 and the adenovirus 5 E1B 55-kD protein. *Genes Dev.* **1994**, *8*, 1235–1246.

(4) Bottger, V.; Bottger, A.; Howard, S. F.; Picksley, S. M.; Chene, P.; Garcia-Echeverria, C.; Hochkeppel, H. K.; Lane, D. P. Identification of novel mdm2 binding peptides by phage display. *Oncogene* **1996**, *13*, 2141–2147.

(5) Bottger, A.; Bottger, V.; Garcia-Echeverria, C.; Chene, P.; Hochkeppel, H. K.; Sampson, W.; Ang, K.; Howard, S. F.; Picksley, S. M.; Lane, D. P. Molecular characterization of the hdm2-p53 interaction. *J. Mol. Biol.* **1997**, *269*, 744–756.

(6) Kussie, P. H.; Gorina, S.; Marechal, V.; Elenbaas, B.; Moreau, J.; Levine, A. J.; Pavletich, N. P. Structure of the MDM2 oncoprotein bound to the p53 tumor suppressor transactivation domain. *Science* **1996**, *274*, 948–953.

(7) Grasberger, B. L.; Lu, T.; Schubert, C.; Parks, D. J.; Carver, T. E.; Koblish, H. K.; Cummings, M. D.; LaFrance, L. V.; Milkiewicz, K. L.; Calvo, R. R.; Maguire, D.; Lattanze, J.; Franks, C. F.; Zhao, S.; Ramachandren, K.; Bylebyl, G. R.; Zhang, M.; Manthey, C. L.; Petrella, E. C.; Pantoliano, M. W.; Deckman, I. C.; Spurlino, J. C.; Maroney, A. C.; Tomczuk, B. E.; Molloy, C. J.; Bone, R. F. Discovery and cocrystal structure of benzodiazepinedione HDM2 antagonists that activate p53 in cells. *J. Med. Chem.* **2005**, *48*, 909–912.

(8) Lai, Z.; Auger, K. R.; Manubay, C. M.; Copeland, R. A. Thermodynamics of p53 binding to hdm2(1−126): effects of phosphorylation and p53 peptide length. *Arch. Biochem. Biophys.* **2000**, *381*, 278–284.

(9) Jabbur, J. R.; Tabor, A. D.; Cheng, X. D.; Wang, H.; Uesugi, M.; Lozano, G.; Zhang, W. Mdm-2 binding and TAF(II)31 recruitment is regulated by hydrogen bond disruption between the p53 residues Thr18 and Asp21. *Oncogene* **2002**, *21*, 7100–7113.

(10) Schon, O.; Friedler, A.; Bycroft, M.; Freund, S. M.; Fersht, A. R. Molecular mechanism of the interaction between MDM2 and p53. *J. Mol. Biol.* **2002**, *323*, 491–501.

(11) Abraham, M. H.; Duce, P. P.; Prior, D. V.; Barratt, D. G.; Morris, J. J.; Taylor, P. J. Hydrogen Bonding. Part 9. Solute Proton Donor and Proton Acceptor Scales for Use in Drug Design. *J. Chem. Soc., Perkin Trans. 2* **1989**, 1355–1375.

(12) Zondlo, S. C.; Lee, A. E.; Zondlo, N. J. Determinants of specificity of MDM2 for the activation domains of p53 and p65: proline27 disrupts the MDM2-binding motif of p53. *Biochemistry* **2006**, *45*, 11945–11957.

(13) Moll, U. M.; Petrenko, O. The MDM2-p53 interaction. *Mol. Cancer Res.* **2003**, *1*, 1001–1008.

(14) Dumaz, N.; Milne, D. M.; Jardine, L. J.; Meek, D. W. Critical roles for the serine 20, but not the serine 15, phosphorylation site and for the polyproline domain in regulating p53 turnover. *Biochem. J.* **2001**, *359*, 459–464.

(15) Craig, A. L.; Burch, L.; Vojtesek, B.; Mikutowska, J.; Thompson, A.; Hupp, T. R. Novel phosphorylation sites of human tumour suppressor protein p53 at Ser20 and Thr18 that disrupt the binding of mdm2 (mouse double minute 2) protein are modified in human cancers. *Biochem. J.* **1999**, *342*, 133–141.

(16) Uhrinova, S.; Uhrin, D.; Powers, H.; Watt, K.; Zheleva, D.; Fischer, P.; McInnes, C.; Barlow, P. N. Structure of free MDM2 N-terminal domain reveals conformational adjustments that accompany p53-binding. *J. Mol. Biol.* **2005**, *350*, 587–598.

(17) Showalter, S. A.; Bruschweiler-Li, L.; Johnson, E.; Zhang, F.; Bruschweiler, R. Quantitative lid dynamics of MDM2 reveals differential ligand binding modes of the p53-binding cleft. *J. Am. Chem. Soc.* **2008**, *130*, 6472–6478.

(18) Vassilev, L. T.; Vu, B. T.; Graves, B.; Carvajal, D.; Podlaski, F.; Filipovic, Z.; Kong, N.; Kammlott, U.; Lukacs, C.; Klein, C.; Fotouhi, N.; Liu, E. A. In vivo activation of the p53 pathway by small-molecule antagonists of MDM2. *Science* **2004**, *303*, 844–848.

(19) Massova, I.; Kollman, P. A. Computational Alanine Scanning To Probe Protein-Protein Interactions: A Novel Approach To Evaluate Binding Free Energies. *J. Am. Chem. Soc.* **1999**, *121*, 8133–8143.

(20) Zhong, H.; Carlson, H. A. Computational studies and peptidomimetic design for the human p53-MDM2 complex. *Proteins* **2005**, *58*, 222–234.

(21) Kortemme, T.; Baker, D. A simple physical model for binding energy hot spots in protein-protein complexes. *Proc. Natl. Acad. Sci. U.S.A.* **2002**, *99*, 14116–14121.

(22) Lee, H. J.; Srinivasan, D.; Coomber, D.; Lane, D. P.; Verma, C. S. Modulation of the p53-MDM2 interaction by phosphorylation of Thr18 - A computational study. *Cell Cycle* **2007**, *6*, 2604–2611.

(23) Dastidar, S. G.; Lane, D. P.; Verma, C. Multiple peptide conformations give rise to similar binding affinities: Molecular simulations of p53-MDM2. *J. Am. Chem. Soc.* **2008**, *130*, 13514–13515.

(24) Zhou, R. H.; Friesner, R. A.; Ghosh, A.; Rizzo, R. C.; Jorgensen, W. L.; Levy, R. M. New linear interaction method for binding affinity calculations using a continuum solvent model. *J. Phys. Chem. B* **2001**, *105*, 10388–10397.

(25) Michel, J.; Verdonk, M. L.; Essex, J. W. Protein-ligand binding affinity predictions by implicit solvent simulations: A tool for lead optimization. *J. Med. Chem.* **2006**, *49*, 7427–7439.

(26) Gilson, M. K.; Zhou, H. X. Calculation of protein-ligand binding affinities. *Annu. Rev. Biophys. Biomol. Struct.* **2007**, *36*, 21–42.

(27) *CHARMM, Version C33b1*; Accelrys, Inc.: San Diego, CA, 2008.

(28) *MacroModel, Version 9.5*; Schrodinger, LLC: New York, NY, 2005.

(29) Guimaraes, C. R. W.; Cardozo, M. MM-GB/SA rescoring of docking poses in structure-based lead optimization. *J. Chem. Inf. Model.* **2008**, *48*, 958–970.

(30) Lyne, P. D.; Lamb, M. L.; Saeh, J. C. Accurate prediction of the relative potencies of members of a series of kinase inhibitors using molecular docking and MM-GBSA scoring. *J. Med. Chem.* **2006**, *49*, 4805–4808.

(31) Espinoza-Fonseca, L. M.; Trujillo-Ferrara, J. G. Transient stability of the helical pattern of region F19-L22 of the N-terminal domain of p53: A molecular dynamics simulation study. *Biochem. Biophys. Res. Commun.* **2006**, *343*, 110–116.

(32) Garcia-Echeverria, C.; Chene, P.; Blommers, M. J. J.; Furet, P. Discovery of potent antagonists of the interaction between human double minute 2 and tumor suppressor p53. *J. Med. Chem.* **2000**, *43*, 3205–3208.

(33) Fasan, R.; Dias, R. L. A.; Moehle, K.; Zerbe, O.; Obrecht, D.; Mittl, P. R. E.; Grutter, M. G.; Robinson, J. A. Structure-activity studies in a family of beta-hairpin protein epitope mimetic inhibitors of the p53-HDM2 protein-protein interaction. *ChemBioChem* **2006**, *7*, 515–526.

(34) *Maestro, Version 8.0*; Schrodinger, LLC: New York, NY, 2005.

(35) *Discovery Studio, Version 2.0*; Accelrys, Inc.: San Diego, CA, 2008.

(36) Sakurai, K.; Schubert, C.; Kahne, D. Crystallographic analysis of an 8-mer p53 peptide analogue complexed with MDM2. *J. Am. Chem. Soc.* **2006**, *128*, 11000–11001.

(37) *Impact, Version 5.0*; Schrodinger, LLC: New York, NY, 2005.

(38) Cheng, Y.; Prusoff, W. H. Relationship between inhibition constant ($K_1$) and concentration of inhibitor which causes 50 percent inhibition (I50) of an enzymatic-reaction. *Biochem. Pharmacol.* **1973**, *22*, 3099–3108.